

---

# Nanoscale Vibrational Analysis of Single-Walled Carbon Nanotubes

## Introduction

Since their discovery in the early 1990s by Iijima,<sup>1</sup> carbon nanotubes have become the focus of intense interest by a vast number of scientists and engineers. The main reason behind such wide-ranging attention lies in their unique electrical,<sup>2</sup> mechanical,<sup>3</sup> thermal,<sup>3</sup> and optical properties.<sup>4</sup> Furthermore, from their size and structure, carbon nanotubes provide a unique system for investigating one-dimensional quantum behavior.<sup>5</sup>

Although many detailed studies have focused on the electronic and mechanical properties of bundles and individual single-walled carbon nanotubes (SWNT's), there has been, to date, no extensive spectral analysis of the properties of SWNT's via their vibrational spectrum on the single-tube level with a spatial resolution of the order of 15 nm. Spectral analysis of individual SWNT's has been carried out in the past,<sup>6</sup> but the techniques used were limited by the inability of conventional confocal microscopy to image and localize nanoscale features with subwavelength resolution.<sup>7–9</sup> Consequently, localized features such as defects or dopants have not been resolved so far. In the work reported here, high-resolution microscopy was performed on individual SWNT's to avoid averaging of the Raman signal. Our unique ability to surpass this limit (i.e., sub-diffraction-limited imaging) lies at the heart of our near-field Raman technique.<sup>10</sup>

Raman spectroscopy is a powerful tool for studying the chemical composition of matter since the energy range of electronic transitions lies within the visible spectrum of electromagnetic radiation. This study focuses on the four main first-order features of SWNT Raman scattering: the radial breathing mode (RBM) ( $\sim 100$  to  $300\text{ cm}^{-1}$ ), the Raman active *D* band ( $\sim 1300\text{ cm}^{-1}$ ), *G* band ( $\sim 1594\text{ cm}^{-1}$ ), and *G'* band ( $\sim 2600\text{ cm}^{-1}$ ).<sup>11–14</sup>

The Raman spectrum can be thought of as a unique chemical fingerprint from which to extract a wealth of information on the electronic structure of SWNT's. For example, the nanotube diameter, chirality, and structure (*n,m*) [(*n,m*) defines the atomic coordinates for the one-dimensional (1-D) unit cell of

the nanotube] are associated with the frequency of the RBM; metallic and semiconducting nanotubes can be distinguished based on the shape of the *G* band (and RBM frequency); and the *D*-band intensity indicates the presence of defects and other disorder-induced effects.

By introducing a sharp gold tip (tip-enhanced Raman spectroscopy<sup>10,15–17</sup>) in the focus of a tightly focused laser beam, the Raman excitation area can be localized to  $\sim 15 \times 15\text{ nm}^2$ . The high spatial frequencies associated with this electromagnetic field confinement allow us to record (near-field) Raman images of SWNT's with a spatial resolution of the order of 10 to 20 nm. Precise spectroscopic information can be extracted as the tip is positioned along a SWNT of interest. In this way unique vibrational maps can be built that show the spatial variation of several Raman active modes along many different SWNT's. We believe that the ability to map spectral changes along SWNT's, with nanoscale precision, will lead to a greater understanding of the fundamental properties of such materials on the single-tube level.

## Experimental Section

Our near-field Raman setup<sup>10</sup> is based on an inverted optical microscope with the addition of an *x,y* stage for raster-scanning samples. Light from a He-Ne laser (633 nm, 50 to 200  $\mu\text{W}$ ) is reflected by means of a dichroic beam splitter and then focused onto the surface of the sample using a high-numerical-aperture objective (N.A. = 1.4).

Having obtained a tight focal spot at the sample surface, a sharp, gold tip is then positioned into the focal region. Care is taken to align the tip with one of the two longitudinal field components in the focal plane.<sup>18</sup> The gold tip is held at a constant height of 1 nm by means of a shear-force detection feedback mechanism<sup>19</sup> with an rms noise of  $\sim 0.5\text{ \AA}$  in the *z* direction. Using the *x,y* stage to raster scan the sample, Raman-scattered light is collected with the same objective and is recorded using either a single-photon-counting avalanche photodiode (APD) or a spectrograph with a charge-coupled device (CCD) cooled to  $-124^\circ\text{C}$ .

SWNT's were grown by the arc-discharge method<sup>3</sup> and purchased commercially. They were then dispersed in a solution of dichloroethane, sonicated in an ultrasonic bath, and spin cast at 3000 rpm onto a glass cover slip. Our metal tips were produced by electrochemically etching thin, gold wire in a solution of hydrochloric acid (HCl) for ~30 s.

## Results

The primary motivation of this study is to probe, with nanoscale resolution, the main vibrational modes of spatially isolated, individual SWNT's; to relate spectral variations to the tube structure (RBM); and to localize defects (*D* band) along the tube axis.

Figure 100.48(a) shows a diffraction-limited, confocal Raman image recorded by raster scanning a sample with a single SWNT through the focused laser. The contrast in the image results from integrating the Raman spectrum for each image pixel over a narrow spectral range centered at  $\nu = 2600 \text{ cm}^{-1}$  (*G'* band). Figure 100.48(b) shows the corresponding near-field Raman image taken over the exact same sample area. This image results from placing a sharp metal tip (25-nm diameter) into the laser focus. The spatial resolution is ~14 nm [full width at half maximum (FWHM)] as shown by the inset of Fig. 100.48(b).

Figure 100.48(c) shows the corresponding Raman-scattering spectrum for a certain nanotube position with and without the tip present. The increase in Raman-scattering strength demonstrates clearly the effect of surface-enhanced Raman scattering (SERS). The SERS enhancement factor depends on the ratio of the near-field and confocal interaction volumes. Typical enhancement factors are in the range of  $10^2$  to  $10^4$  (Ref. 10).

In the next step, a sample area was located with single nanotubes that show detectable signals for all four Raman active bands. Figures 100.49(a)–100.49(d) show a series of near-field spectral images of two individual SWNT's corresponding to the *G*, *G'*, *D*, and RBM Raman bands.

From these images one can clearly observe the spatial variation in Raman-scattered light for all four Raman bands. Both the *G* and *G'* bands [Figs. 100.49(a) and 100.49(b)] show a near-uniform-intensity profile along the nanotube in the center of the image, as one might expect for a defect-free SWNT. This observation is further strengthened by the weak intensity of the disorder-induced *D* band [Fig. 100.49(c)]. The most striking spectral feature is the localized scattering associated with the RBM. Figure 100.49(d) illustrates that only one nanotube, namely the SWNT in the center of the image, is

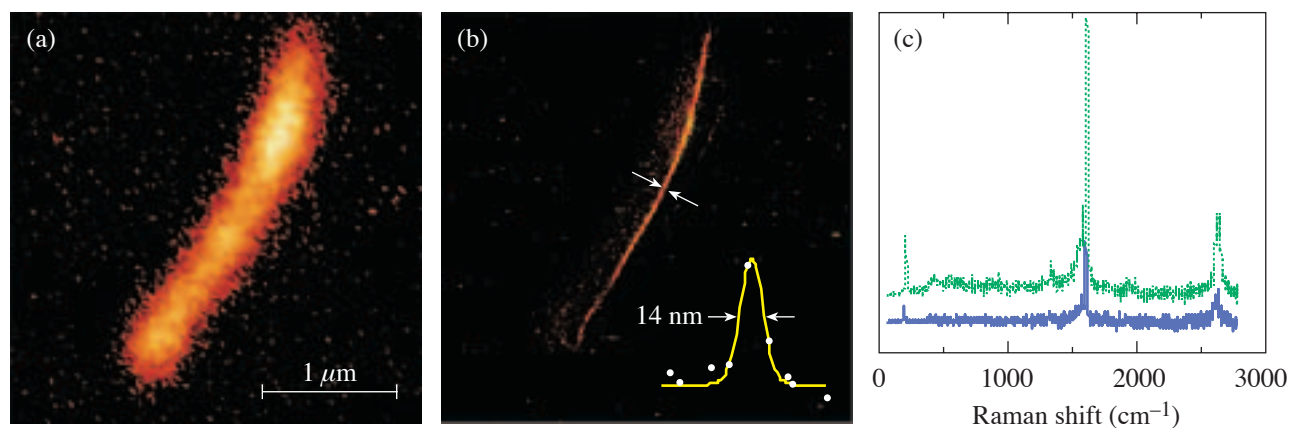


Figure 100.48

[(a) and (b)] Raman-scattering images of a single SWNT deposited on a glass coverslip. The contrast in the images reflects the local intensity of the Raman *G'* band:  $2600 \text{ cm}^{-1}$ . (a) A confocal Raman image and (b) the corresponding near-field Raman image. The integration time was 10 ms per image pixel. The inset in (b) shows a Gaussian fit to the line section shown (FWHM of 14 nm). The FWHM taken from (a) was ~275 nm. (c) Raman-scattering spectrum for a single SWNT with (upper) and without (lower) a metal tip present. The graphs are offset for clarity.

resonantly excited with our light source. The detected RBM frequency was measured to be  $\sim 205\text{ cm}^{-1}$ , indicating that we observe a (14,1) nanotube. Using the relation  $\nu_{\text{RBM}} = A/d_t + B$ , (where  $A = 223.5\text{ nm/cm}$  and  $B = 12.5\text{ cm}^{-1}$ ),<sup>14</sup> we calculate the tube diameter to be  $1.16 \pm 0.2\text{ nm}$ . Atomic force microscopy (AFM) measurements confirm that it is indeed a single nanotube, its diameter being measured topographically to be  $\sim 1.3\text{ nm} \pm 0.3\text{ nm}$ .

To understand the origin of these local variations, we first discuss the resonance conditions associated with the different Raman bands. The RBM resonance window is different compared to the resonance windows for the  $G$ ,  $G'$ , and  $D$  Raman modes.<sup>7</sup> The RBM is more likely to change in the presence of

nanotube defects, such as localized changes in the structure of the nanotube lattice [changes in  $(n,m)$ ], kinks, and intertube junctions in addition to interactions with the glass substrate on which the SWNT's are dispersed. Any of these variations will affect the van Hove transition energy  $E_{ii}$  and detune the RBM out of resonance. For the  $G$ ,  $G'$ , and  $D$  Raman active bands respectively, any small change in  $E_{ii}$  is unlikely to manifest itself in similarly dramatic spectral variations.

The dispersive  $G$ ,  $G'$ , and  $D$  bands are discussed in terms of a double resonance effect that relaxes the resonance condition.<sup>12</sup> On the other hand, the RBM originates from a single resonance process, resulting in a slightly narrower resonance window.<sup>13</sup> Since the resonance windows for the Raman active  $G$  and  $G'$  bands are broader in nature, dramatic spectral changes are not as expected, as can be seen in Figs. 100.49(a) and 100.49(b). However, as will be reported in a later publication, we have observed significant spectral variations, on the single-tube level, in the  $G$  and  $G'$  Raman bands for SWNT's that have been doped with elemental boron.<sup>20</sup>

Figure 100.49(c) reveals the presence of a small amount of scattered light associated with the Raman  $D$  band centered at  $1267\text{ cm}^{-1}$ . In light of the weak signal associated with this band, we relate such scattering to disorder-induced effects within the tube lattice itself or the coupling to the supporting substrate. In a related study on boron-doped tubes, we have observed significant increases of  $D$ -band scattering, localized with 20-nm resolution, along several different SWNT's.<sup>20</sup>

In light of our work, it should be noted that recent experiments on SWNT's suspended from Si pillars have shown Raman signals that are more intense when compared to SWNT's in contact with a silicon surface;<sup>21</sup> however, no localized spectral analysis has been reported so far for suspended SWNT's. The ability to perform such localized analysis of suspended SWNT's should provide a better understanding of the effects of nanotube–surface interactions on the variations of the vibrational modes of SWNT's.

Our observation and explanation of the RBM localization are consistent with the results that we acquired for many different tube structures (assigned from RBM frequency). Figures 100.50(a)–100.50(e) show further evidence for localized Raman scattering associated with the following Raman active modes: namely, (a) the  $G$  band, (b)  $D$  band, (c) RBM, (d) intermediate-frequency modes (IFM),<sup>13</sup> and (e)  $M$  band.<sup>22</sup> Figure 100.50(f) shows a three-dimensional AFM profile of the nanotube studied.

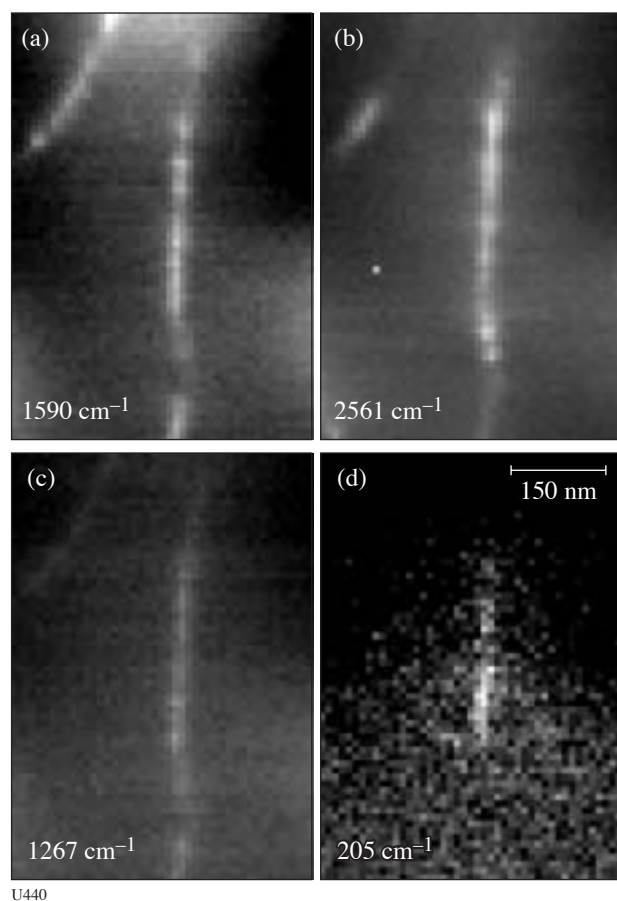


Figure 100.49  
Near-field spectral images, upon laser excitation at 633 nm, for the Raman active (a)  $G$  band, (b)  $G'$  band, (c)  $D$  band, and (d) RBM. The images were produced from the Raman-scattered light detected with a cooled CCD. (Integration time: 210 ms per image pixel.) The most-striking feature is the localization of the RBM associated with the vertically aligned SWNT.

Once again localized spectral variations of the RBM are observed. The RBM signal decreases dramatically in the presence of  $\sim 3$ -nm-high catalyst particles located at the tube's end. This observation is consistent with the idea that changes in the tube structure can lead to a loss of resonance Raman-scattering properties of SWNT's. From Fig. 100.50(b) considerable *D*-band scattering is also observed at the beginning of the tube, where a small kink is present, and near the end with the small catalyst particles. The vibrational modes shown in Figs. 100.50(d) and 100.50(e) are recorded along a single

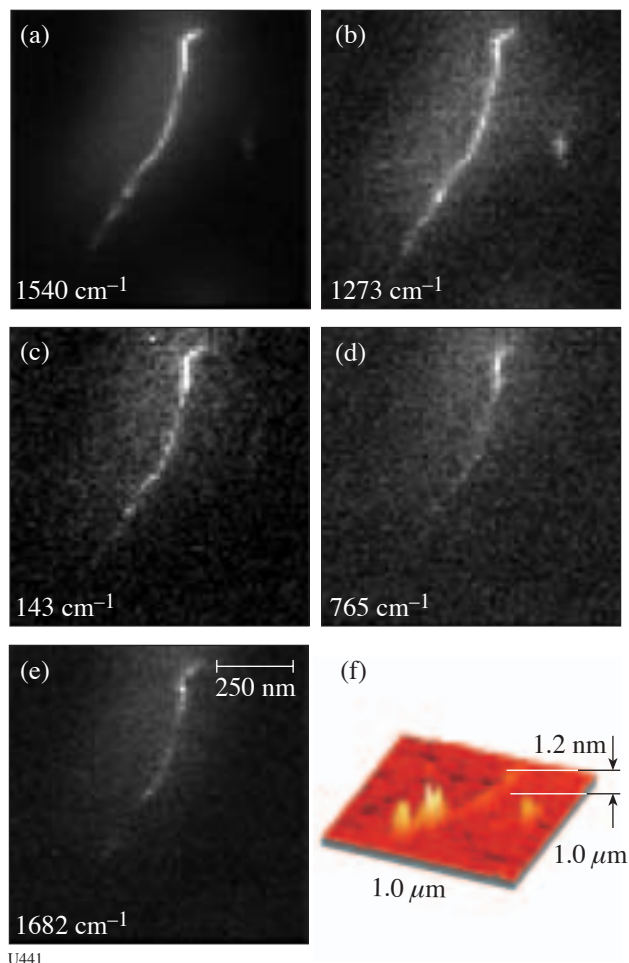


Figure 100.50

[(a)–(e)] Near-field spectral images for different Raman bands. (f) A 3-D topographical profile of the nanotube studied. Two bands previously unseen in our SWNT studies are (d) an intermediate-frequency mode (IFM)<sup>13,23</sup> and (e) the Raman active *M* mode.<sup>22</sup> Again the presence of a spatially varying RBM along the nanotube length is observed. The RBM, as well as the IFM and *M* bands, decrease in strength near the attached  $\sim 3$ -nm particle(s), which is presumably a residual Ni/Y catalyst particle left over from the growth process.

nanotube for the first time. The two bands are designated as an intermediate frequency mode (IFM) and *M* band, respectively, and are known from the literature.<sup>13,22</sup> The *M* band is the sum of the RBM and the *G* band, although it should be noted that the *M* band also appears in the Raman spectrum of graphite. Our calculations show that subtracting the frequency of the *G* band from the *M* band gives  $142\text{ cm}^{-1}$ . This is consistent with the measured value of the RBM frequency:  $143\text{ cm}^{-1}$ . From this measured RBM frequency we assign a nanotube structure of (23,1); i.e.,  $(n,m) = (23,1)$ . To the best of our knowledge, no previous attempt has been made to understand why both the IFM and *M* modes are localized similar to the observed spatial variations of the RBM. We conclude that both the IFM and *M* band are dependent on the tube structure  $(n,m)$  in the same manner as the RBM. This claim is strengthened by the fact that these bands are not always detectable for either SWNT bundles or individual SWNT's. Future work should provide more-detailed insight into the spatial variation of these two bands and any possible dependence on the tube diameter, i.e.,  $(n,m)$ .

For all near-field Raman images, a topographic image (not shown in Figs. 100.48 and 100.49), acquired simultaneously, provides a valuable crosscheck for the  $(n,m)$  assignments based on the RBM frequency. All SWNT's studied had their diameters calculated from the spectral position of their (diameter-dependent) RBM frequencies. The calculated value was then compared with the corresponding AFM measurements to confirm that they were, indeed, individual SWNT's and not small bundles. In addition, the same gold tip was used to acquire all of the images shown.

## Conclusion

In conclusion, using near-field Raman imaging and spectroscopy, several vibrational modes have been mapped along spatially isolated, individual SWNT's resting on a glass substrate with 20-nm resolution. Our results demonstrate that high-resolution microscopy is necessary to avoid averaging of the Raman spectrum along individual SWNT's. As such, our results reveal the highly localized nature of the light scattering associated with the RBM frequency from several different SWNT's. Such spectral features are ascribed to the sensitive nature of the RBM resonance condition. Variations in the RBM scattering are attributed to the surrounding environment (nanotube–substrate interactions) and its effect on the nanotube structure  $(n,m)$  and hence transition energy  $E_{ij}$ . Furthermore, little variation in intensity has been observed for both the *G* and *G'* Raman bands. Such small variations result from the different resonance conditions for these bands in comparison with the resonance window of the RBM for SWNT's. Finally,

detectable Raman scattering associated with disorder-induced effects has been observed; however, for many perfectly aligned SWNT's, little or no *D*-band intensity has been detected.

#### ACKNOWLEDGMENT

The authors wish to thank Dr. A. Bouhelier and Dr. A. Jorio for stimulating discussions and T. Osedac for tip fabrication. This research has been supported financially by the Air Force Office for Scientific Research (AFOSR) through the Multidisciplinary University Research Initiative (MURI) under Grant No. F-49620-03-1-0379.

#### REFERENCES

1. S. Iijima, *Nature* **354**, 56 (1991).
2. M. T. Woodside and P. L. McEuen, *Science* **296**, 1098 (2002).
3. M. S. Dresselhaus, G. Dresselhaus, and P. Avouris, *Carbon Nanotubes: Synthesis, Structure, Properties, and Applications*, Topics in Applied Physics, Vol. 80 (Springer, Berlin, 2001).
4. A. Hartschuh *et al.*, *Science* **301**, 1354 (2003).
5. L. C. Venema *et al.*, *Science* **283**, 52 (1999).
6. A. Mews *et al.*, *Adv. Mater.* **12**, 1210 (2000).
7. M. Souza *et al.*, *Phys. Rev. B* **69**, 241403(R) (2004).
8. K. McGuire *et al.*, "Synthesis and Raman Characterization of Boron-Doped Single-Walled Carbon Nanotubes," submitted to *Physical Review B*.
9. S. B. Cronin *et al.*, *Phys. Rev. Lett.* **93**, 167401 (2004).
10. A. Hartschuh *et al.*, *Phys. Rev. Lett.* **90**, 095503 (2003).
11. A. Jorio *et al.*, *Phys. Rev. Lett.* **86**, 1118 (2001).
12. S. Reich, C. Thomsen, and J. Maultzsch, *Carbon Nanotubes: Basic Concepts and Physical Properties* (Wiley-VCH, Cambridge, England, 2004).
13. A. M. Rao *et al.*, *Science* **275**, 187 (1997).
14. S. W. Bacilo *et al.*, *Science* **298**, 2361 (2002).
15. J. Wessel, *J. Opt. Soc. Am. B* **2**, 1538 (1985).
16. N. Hayazawa *et al.*, *Chem. Phys. Lett.* **335**, 369 (2001).
17. R. M. Stöckle *et al.*, *Chem. Phys. Lett.* **318**, 131 (2000).
18. L. Novotny, E. J. Sánchez, and X. S. Xie, *Ultramicroscopy* **71**, 21 (1998).
19. K. Karrai and R. D. Grober, *Appl. Phys. Lett.* **66**, 18424 (1995).
20. N. Anderson *et al.*, in preparation.
21. Y. Kobayashi *et al.*, *Chem. Phys. Lett.* **386**, 153 (2004).
22. V. W. Brar *et al.*, *Phys. Rev. B* **66**, 155418 (2002).
23. In a recent article C. Fantini *et al.* discuss the origin of IFM's for many different laser wavelengths. See *Phys. Rev. Lett.* **93**, 087401 (2004) for further details.

